HHS Public Access

Author manuscript

J Magn Reson Imaging. Author manuscript; available in PMC 2019 August 01.

Published in final edited form as:

J Magn Reson Imaging. 2018 August ; 48(2): 431–440. doi:10.1002/jmri.25936.

Improved Detection of fMRI Activation in the Cerebellum at 7T with Dielectric Pads Extending the Imaging Region of a Commercial Head Coil

M. V. Vaidya, PhD[1,2], **M. Lazar, PhD**[1,2], **C. M. Deniz, PhD**[1], **G. G. Haemer, MS**[1,2], **G. Chen, PhD**[1,2], **M. Bruno, BS**[1], **D. K. Sodickson, MD PhD**[1,2], **R. Lattanzi, PhD**[1,2], and **C. M. Collins, PhD**[1,2]

[1]Center for Advanced Imaging Innovation and Research (CAI[2]R) and Bernard and Irene Schwartz Center for Biomedical Imaging, Department of Radiology, New York University School of Medicine, 660 1st Avenue. New York, NY 10016, USA

[2]The Sackler Institute of Graduate Biomedical Sciences, New York University School of Medicine, 550 1st Avenue, New York, NY 10016, USA

Abstract

BACKGROUND—There is growing interest in detecting cerebro-cerebellar circuits, which requires adequate BOLD contrast and signal-to-noise ratio (SNR) throughout the brain. Although 7T scanners offer increased SNR, coverage of commercial head coils is currently limited to the cerebrum.

PURPOSE—To improve cerebellar fMRI at 7T with high permittivity material (HPM) pads extending the sensitivity of a commercial coil.

STUDY TYPE—Simulations were used to determine HPM pad configuration and assess RF safety. In vivo experiments were performed to evaluate RF field distributions and SNR and assess improvements of cerebellar fMRI.

SUBJECTS—Eight healthy volunteers enrolled in a prospective motor fMRI study with and without HPM.

FIELD STRENGTH/SEQUENCE—Gradient echo EPI for fMRI, turbo FLASH for flip angle mapping, GRE sequence for SNR maps, and T_1-weighted MPRAGE were acquired with and without HPM pads at 7T.

ASSESSMENT—Field maps, SNR maps, and anatomical images were evaluated for coverage. Simulation results were used to assess SAR levels of the experiment. Activation data from fMRI experiments was compared with and without HPM pads.

STATISTICAL TESTS—fMRI data were analyzed using FEAT FSL for each subject followed by group level analysis using paired t-test of acquisitions with and without HPM.

CORRESPONDING AUTHOR: Christopher M. Collins, The Bernard and Irene Schwartz Center for Biomedical Imaging, New York University Langone Medical Center, 660 First Avenue – Fourth Floor, New York, NY 10016, USA, tel: (+1)-212-263-4860, fax: (+1)-212-263-7541, c.collins@nyumc.org.

RESULTS—Simulations showed 52% improvement in transmit efficiency in cerebellum with HPM and SAR levels well below recommended limits. Experiments showed 27% improvement in SNR in cerebellum and improvement in coverage on T_1-weighted images. fMRI showed greater cerebellar activation in individual subjects with the HPM pad present (Z>=4), especially in inferior slices of cerebellum, with 59% average increase in number of activated voxels in the cerebellum. Group-level analysis showed improved functional activation (Z>=2.3) in cerebellar regions with HPM pads without loss of measured activation elsewhere.

DATA CONCLUSIONS—HPM pads can improve cerebellar fMRI at 7T with a commonly-used head coil without compromising RF safety.

Keywords

fMRI; cerebellum; High permittivity materials; brain imaging; SAR; SNR

INTRODUCTION

Functional magnetic resonance imaging (fMRI) has facilitated non-invasive in vivo studies of brain function and connectivity for various task-based and resting state paradigms (1-3). Although the vast majority of studies have been concerned with activity in the cerebral cortex, there is a growing interest in structural and functional imaging of the cerebellum (4,5). There is, in particular, an interest in studying the functional role of cerebro-cerebellar circuits (4-7), which require robust sensitivity to blood oxygenation level dependent (BOLD) contrast throughout the whole brain.

It is well known that fMRI at 7T can provide much better sensitivity to fMRI activation compared to lower field strengths (8,9). This can be used to improve spatial resolution and reduce the number of trials (9,10) required to detect cerebellar cortex and small sized deep cerebellar nuclei activation in various task based functions (9-11). However, the variety of radiofrequency (RF) coils commercially available for imaging at 7T is still limited, due in part to the technical challenges associated with higher operating frequencies, such as inhomogeneity of the RF field used in excitation and asymmetric transmit and receive RF field patterns for surface coils (12-14). The commercial coils used most often for brain imaging at 7T today are designed primarily for imaging the cerebrum with a steep gradient in signal often seen in the cerebellum and other inferior regions of the head (15,16).

The most commonly used commercially available 7T head coil consists of a relatively short transmit birdcage coil surrounding a receive array (Nova Medical, Wilmington, MA). This coil is designed primarily for imaging the cerebrum with a limited field-of-view (FOV) relative to commercial head coils used at lower field strengths, where excitation is often accomplished with the system's large whole-body birdcage coil.

The use of high permittivity material (HPM) (relative permittivity $\varepsilon_r > 50$) pads in MRI has been proposed to improve SNR, increase transmit efficiency, and reduce excitation inhomogeneity (17-21). These advantages are attributed to displacement currents within the dielectric pad that add to the local magnetic field according to the modified Ampere's law (19). Recently, materials with a relative permittivity of greater than 100 have been

constructed from calcium or barium titanate powders mixed with deuterium oxide for greater benefit in MRI applications (22,23).

A variety of studies have been conducted using HPM in conjunction with a commercial head coil at 7T (15,22-27). Haines et al. demonstrated that positioning HPM pads on one or both sides of the head can improve signal homogeneity and SNR in the temporal lobes of the cerebrum (22). Shortly thereafter Snaar et al. characterized improvements in MR spectroscopy with this arrangement (24) and Teeuwisse et al. characterized this improvement in SNR along the sides of the head and brain with pads placed to the left and right sides of the head with more quantitative experimental measures (25) and simulations (23). Teeuwisse et al. also showed that positioning water pads along the left and right side of the head extending down to the neck during an arterial spin labeling sequence increased the strength of the excitation field (B_1^+) in the carotid artery, and improved the SNR in brain perfusion maps at 7T (15). Although this arrangement of an HPM pad on either side of the head also showed improved excitation, SNR, and coverage in the anterior portion of the cerebellum, seen on a coronal plane through the midbrain, it resulted in a strong RF field gradient across the cerebellum in the anterior-posterior direction. This RF field gradient resulted in both lower excitation and SNR in the posterior cerebellum when the HPM pads were present (25). A different arrangement with HPM pads against the inferior, posterior portion of the head showed improvement in inversion efficiency and coverage of the whole brain using MP2RAGE scans in combination with low B_1^+ adiabatic pulses (26). This study presented improvement in image quality in the cerebellar region with no quantitative measures of SNR.

The aim of this work is to improve cerebellar fMRI using a commercial head coil at 7T. To accomplish this, we arrange HPM pads against the inferior, posterior portion of the head. We first investigate the technical potential of using HPM to improve SNR throughout the cerebellum without increase in hazard due to RF heating (Specific energy Absorption Rate or SAR) in simulations, then examine the effects on available SNR as well as measured fMRI activation throughout the brain (including the cerebellum) during a finger-tapping task in eight subjects.

MATERIALS AND METHODS

Simulations

We performed numerical simulations to determine the appropriate material properties of the HPM pads, evaluate the changes in the electromagnetic field within the head model with HPM pads, examine changes in the scattering (S) parameters of the transmit coil, and assess the simulated local and global SAR values. HPM pads were modeled with properties that are achievable using mixtures of powder and water slurries made with barium titanate ($BaTiO_3$, $\varepsilon_r = 298$, $\sigma = 0.39$ S/m) or calcium titanate ($CaTiO_3$, $\varepsilon_r = 110$ and $\sigma = 0.08$ S/m) (22,23). To closely match experiments, the electrical properties of the mixtures for the simulations were determined by experimentally measuring the properties of saturated mixtures of titanate powders with deuterium oxide using a dielectric probe as described in the following section.

A head-sized quadrature-driven birdcage coil, similar to the transmit head coil used in the experiments (Fig. 1), was modeled using CST Microwave Studio 2015 (Computer Simulation Technology, Darmstadt, Germany), and loaded with a human model ("Duke," Virtual Population, IT'IS Foundation, Zurich, Switzerland) (28) with a voxel resolution of 5 × 5 × 5 mm^3. Each port was tuned to 297.2 MHz, the operating frequency of our 7T MR scanner, and matched to 50 Ohms in the absence of HPM. Note that the receive coils were not modeled in the simulation.

Two HPM pads (12 × 14 × 2 cm^3) were modeled from sections of spherical and cylindrical shells and positioned at the base of the skull such that they extended 7 cm from the coil as shown in Figure 1. The properties of both pads were the same for each case. The birdcage coil was not re-tuned and re-matched in the presence of the HPM pads, as tuning and matching was fixed for the commercial coil used in the experiments. Simulations were performed with an accuracy of −30 dB to ensure convergence, and approximately 14 million mesh cells were used with the same global (lines per wavelength = 25, lower mesh limit = 20, mesh line ratio limit = 20) and local (mesh size of PVC layer covering HPM = 1 × 1 × 1 mm^3) mesh settings for all cases. Transmit efficiency ($\left|B_1^+\right|/\sqrt{P}$, where B_1^+ is the transmit field and P is the input power) was evaluated for three cases: No HPM, $BaTiO_3$ pads, and $CaTiO_3$ pads (Fig. 2).

To compare the SAR values to the safety limits prescribed by the Food and Drug Administration (FDA) (29) and the International Electrotechnical Commission (IEC) (30), the SAR values obtained in the CST simulation environment were scaled (31) to correspond to the gradient-echo EPI sequence used in experiments as follows.

We considered a target $|B_1^+|$ of 3 μT, which corresponds to a 90 degree flip angle with a rectangular pulse having a duration of approximately 2 ms. To normalize fields and SAR to this target $|B_1^+|$ strength, first the target $|B_1^+|$ was divided by the average simulated $|B_1^+|$ in the center or in the cerebellum for cases with and without HPM. This ratio was squared (since SAR is proportional to the square of electric field and magnetic field strengths) and the resulting scaling factor was multiplied by the peak local 10 g SAR obtained from simulations with constant input power. This instantaneous SAR, now corresponding to that during a rectangular pulse producing a flip angle of 90 degrees and having a duration of 2 ms, was then scaled to include a TR of 3000 ms, a pulse duration of 2 ms and 55 slices (31). To calculate the simulated head-average SAR, the power dissipated in the tissue was scaled by the same scaling factor as above and divided by 5 kg, which is approximately the mass of the head.

Experiments

The electrical properties of the HPM pads used in simulations were determined by mixing either $CaTiO_3$ powder (Alfa Aesar, 99 +%, −325 mesh powder) or $BaTiO_3$ powder (Sigma Aldrich, 99 %, powder, < 3 μm) with deuterium oxide (Sigma Aldrich, 99 atom % D) to obtain a saturated slurry. The electrical properties of the saturated slurries were measured (85070E Dielectric Probe Kit, Agilent Technologies, Santa Clara, CA, USA) to be $\varepsilon_r = 110$ and $\sigma = 0.08$ S/m for $CaTiO_3$ slurry and $\varepsilon_r = 298$, $\sigma = 0.39$ S/m for $BaTiO_3$ slurry.

Since simulation results showed that calcium titanate was more advantageous than barium titanate, we constructed HPM pads using the $CaTiO_3$ slurry. The HPM slurry was then heat-sealed between plastic sheets to create two pads with approximate dimensions 12 × 14 × 2 cm^3.

All studies involving human subjects were performed in accordance with the institution's IRB. Informed research consent was obtained for all subjects. Volunteers were scanned on a whole-body 7T scanner (Magnetom, Siemens Healthineers, Erlangen, Germany) using a commercial head coil with one transmit channel and 24 receive channels (Nova Medical, Wilmington, MA). Either the HPM pads or conventional foam pads were placed inside the coil (Fig. 1), such that approximately 7 cm of the longest dimension extended outside the coil. For each volunteer, the transmit reference voltage was set with no HPM inside the coil such that a 90° flip angle was achieved at the center of the brain, corresponding to the coil center. Flip angle maps were obtained with a turbo-FLASH based technique (32). The transmit voltage was then kept constant for the volunteer's session with HPM.

To assess the coil performance with and without HPM pads, SNR maps were acquired for one volunteer. SNR maps were generated using the raw data from two gradient echo acquisitions (TR/TE = 200/4.1 ms, nominal FA = 20°, BW = 300 Hz/pixel, FOV = 285 × 285 mm^2, matrix size = 256 × 256), one with and the other without RF excitation (33). Flip angle maps obtained during the same session were normalized to account for the nominal flip angle used in the GRE sequence for calculating SNR maps. To evaluate receive-signal contribution to SNR, the SNR maps were then divided by the sine of the corresponding normalized flip-angle map.

fMRI experiments

To assess the BOLD contrast improvement with HPM in the cerebellum, where the SNR and $|B_1^+|$ distribution is inherently poor for the particular coil used, BOLD contrast weighted scans were acquired for eight healthy volunteers (four male, four female; mean age = 31.4, standard deviation = 6.57).

fMRI experiments with and without HPM pads were completed using a gradient echo EPI sequence (101 measurements, axial slices=55, voxel size = 2 × 2 × 2.5 mm^3, TR=3 s, TE=23 ms, band width = 1930 Hz/pixel, flip angle = 15deg). Flip angle maps were obtained with a turbo-FLASH based technique (32) to set the transmit reference voltage. For each volunteer, two fMRI scans were acquired: one without and one with the HPM pads. To ensure $\boldsymbol{B}_0$ homogeneity in the whole brain a 3D volume shim was carried out prior to each EPI acquisition. In addition, T_1-weighted MPRAGE images (TR=2250 s, TE=3.32 s, TA=5.14 min, resolution =1×1×1mm^3, flip angle= 8°) were obtained for registration with the functional data.

For the functional paradigm, volunteers were asked to carry out a finger tapping task using the right hand. Prior to the scans, volunteers were briefly trained outside of the scanner. A simple block design was used with six active and six rest blocks with each block (24 s each) consisting of eight measurements (3 s each) for a total of 101 measurements.

Statistical analysis

Data were analyzed using FEAT (fMRI Expert Analysis Tool, version 6.0), which is a part of FSL (FMRIB's software Library, www.fmrib.ox.ac.uk/fsl, version 5.0.10). Non-brain removal for the T_1-weighted images for all cases was carried out with brain extraction tool (BET). Pre-processing of the BOLD data included discarding the first five measurements to ensure achieving steady-state excitation, high pass filtering (with a cut-off of 48 s), motion correction using MCFLIRT, spatial smoothing using a Gaussian kernel of FWHM 5mm and interleaved slice timing correction. Registration was first carried out to the respective T_1-weighted image and then to the MNI standard space image, using FLIRT. Z (Gaussianised T/F) statistic images were thresholded with Z > = 2.3 and a corrected cluster significance threshold of P = 0.05. The total number of voxels with a threshold of Z = 6 and maximum Z value within the cerebellum for cases with and without HPM for each subject were calculated using the cluster function in FSL.

To assess whether the BOLD contrast improved with HPM over the entire population from which the volunteers were sampled, a higher level analysis was carried out at group level using a paired t-test of the two acquisitions: with and without HPM for the same 8 subjects. Higher level statistical modeling was carried out using mixed effects with FLAME 1 (FMRIB's Local Analysis of mixed effects) in FEAT with a Z threshold = 2.3.

RESULTS

In the presence of HPM, simulated S_{11} for all 4 ports of the transmit coil remained below –20 dB, except for S_{33} (−16.93 dB) and S_{44} (−18.14 dB) with $CaTiO_3$, and S_{44} (- 19 dB) with $BaTiO_3$. S_{21} values did not change by more than 2 dB. As an increase of 3 dB from –20 dB, for S_{11}, translates into an insignificant increase in reflected power to 2 % from 1 % of transmitted power, re-matching and re-tuning the birdcage component of the head coil would not substantially improve transmit efficiency. Additionally, a maximum change in S_{21} by 2 dB translates to a negligible change in the degree of circular polarization of the transmit coil. RF data from the scanner for one volunteer showed that the forward and reflected power did not change significantly with the addition of the HPM (% power reflected of forward power without HPM = 1.6 % and with HPM = 1.2 % for an EPI sequence).

The simulated transmit efficiency improved in both the superficial and the deep regions of the posterior head and neck when calcium titanate was used for the HPM pads (Fig. 2 B). For the case with barium titanate (Fig. 2 C), transmit efficiency was degraded in deeper regions of the head and neck, as compared to the case without HPM (Fig. 2 A). In the absence of HPM pads the resultant flip angle in the cerebellum would be approximately half that in the central region (Fig 2A). For example, a pulse producing a 90° excitation in the cerebellum would produce a 171° excitation in the central region when no pad is present. Therefore, all experiments were performed using HPM pads made with $CaTiO_3$ slurries (Fig. 1 B). Transmit efficiency increased by 52 % on average in the cerebellum (outlined in Fig. 2) and decreased by 7.3 % in the coil center (outlined in Fig. 2) with $CaTiO_3$ pads.

Maximum 10 g local and head average SAR values from the simulation were scaled to correspond to the EPI sequence used either for a target 90° in the coil center or in the

cerebellum (Table 1). All resulting SAR values were well below the corresponding limits (10 W/kg for maximum local SAR and 3.2 W/kg for head average SAR) recommended by the FDA and IEC (29,30). The presence of HPM pads reduced the resultant SAR values by more than 50 % for a target excitation of 90° in the cerebellum.

Experimental SNR maps showed an overall distribution change in the presence of the HPM pads (Fig. 3). The HPM pads improved the SNR by 27 % in the cerebellum (outlined in white). SNR maps normalized by the excitation flip angle maps resulted in a 7.2 % reduction in the receive-only SNR in the cerebellum, suggesting that the improvement in the SNR is primarily due to the increase in the flip angle (by 38.6 %) with HPM.

The spatial distribution of the flip angle maps in the experiments showed a similar trend to simulations, with improved performance towards the base of the skull (including cerebellum) when the $CaTiO_3$ pad is present (Fig. 4 vs. Fig 2). The flip angle averaged across all subjects showed a mean improvement of 33 % in the cerebellum and a decrease of 3.4 % at the center, while the average flip angle in the whole brain remained approximately the same (see ROIs in Fig 4).

The T_1-weighted MPRAGE images in Fig. 5 show improved visibility of the cerebellum, the cervical vertebrae, the spinal cord, the brainstem, and the superficial neck muscles in the presence of the calcium titanate pads.

Functional MR images show contralateral motor cortical activation and activation of the superior and inferior axial slices of the ipsilateral cerebellar cortex. In the presence of HPM pads, a statistically significant improvement in the functional activation was observed for the inferior axial slices of the cerebellum (Fig. 6).

The total number of activated voxels within the cerebellum was higher with HPM in all but one subject, with an increase in all subjects ranging from −7 to 153 % (Table 2). Maximum Z value also increased for all but one subject (Table 2). Group analysis results show a statistically significant increase in activation in the cerebellar cortex with the HPM (Fig. 7), which corresponds to the position of the calcium titanate pads near the neck of the subjects (Fig. 1), and with no considerable loss elsewhere in the brain.

DISCUSSION

This work demonstrated, in both simulation and experiment, that the sensitivity of a standard commercial 7T head coil can be improved in the cerebellum and regions inferior to the base of the skull using HPM pads extending out of the coil. This gain in SNR was utilized for improving functional imaging of the whole brain including the cerebellum, where the commercial coil on its own suffered from poor transmit and receive sensitivity.

Maximum local SAR and global SAR decreased with HPM when producing a constant $|B_1^+|$ in the cerebellum, but increased when producing a constant $|B_1^+|$ in the coil center. As shown in previous work (34), our results also indicate that in the presence of HPM pads a lower SAR can be obtained when calibrating for a specific transmit flip angle in a specific ROI, provided that transmit efficiency gains with HPM are achieved in that ROI. In our

experiments we chose to keep the input power constant between the cases with and without HPM to minimize variables in evaluating the functional activation throughout the whole brain. As the mean experimental flip angle and simulated transmit efficiency in the center of the head did not change considerably with HPM, SAR values scaled for target $|B_1^+|$ in the center of the head approximated our experimental setup. The decrease in receive-only sensitivity in the cerebellum indicates that the improvement in SNR, for our experimental setup, is primarily from the increase in the flip angle in the cerebellum with HPM. However, simply increasing the voltage in the absence of HPM to increase the flip angle in the cerebellum would not provide the same benefit as with HPM: the inherently poor transmit efficiency in the cerebellum dictates that increasing the voltage for a desired flip angle in the cerebellum would result in overtipping in other regions (with almost double the desired flip angle in the center of the brain) and in much higher SAR levels.

Although the scaled maximum 10g local and head average SAR values for an EPI sequence like we used in experiment increased with addition of the HPM when maintaining a target $|B_1^+|$ at the coil center, they were both well below limits recommended by the FDA and IEC (29,30). Due to the low SAR of the fMRI sequence in general, SAR would also be below the recommended limits even if no HPM were used and the pulses were defined to produce optimal excitation in the cerebellum. In this case, the presence of HPM pads would reduce SAR values, demonstrating an inherent benefit of using HPM pads when optimizing excitation in ROIs in close proximity to the pads. Note that neither the IEC nor the FDA suggests limits on maximum local SAR for volume coils, but we evaluated maximum 10 g SAR because the effect of HPM is more localized in nature. Because a standard EPI sequence is inherently low in SAR, similar analysis should be performed before use of more SAR-intensive sequences. The precise pulse duration and pulse shape of the experimental sequence were not available from the scanner, but 2 ms rectangular pulses were used as reasonable estimates.

Our results are consistent with other studies that demonstrated an SNR advantage with strategic use of HPMs (19,24,34-36). In addition to a higher SNR in the cerebellum when using HPM pads, we also observed higher SNR in the neck muscles. SNR and flip angle map results were consistent with the T_1 weighted MPRAGE images, which showed improved visibility of the neck muscle, brainstem and spinal cord, vertebral bodies, and cerebellum. These images also showed ample signal and contrast in the areas with a decrease in SNR, including the frontal and central regions of the brain. The experimental SNR maps normalized by the sine of the flip angle also demonstrated that the improvement in SNR achieved was primarily due to the transmitted flip angle and not the received-signal for the particular head coil used.

Improvement in measured functional activation with HPM pads indicates that the gain in transmitted flip angle achieved using HPM pads translates directly to improved measurement of BOLD contrast. Table 2, in particular, shows that not only did the cerebellar activation (maximum Z value) improve using HPM pads, but the total number of activated voxels also increased. The functional activation pattern was in agreement with previous studies that showed a functional topography specifically in the ipsilateral anterior (lobules V, and VI) and posterior (VIII) lobules of the cerebellum (4,11). We anticipate that other tasks

based on language, which have been shown to map onto intermediate lobule VI and Crus I (4), or cognitive tasks shown to map to Crus II and lobule VII (5), would also show larger cerebellar activation with HPM pads. The SNR increase with HPM could also provide advantages in studies of the functional role of small structured nuclei in the cerebellum, such as the dentate nucleus, in order to improve the low thresholds for quantifying functional activation and resolution for structural imaging (11,37).

Our work focused on using HPM in conjunction with a commercial head coil to improve the FOV for whole-brain fMRI at 7T by improving the transmit efficiency in the cerebellum. The particular positioning of the HPM pads not only extended the FOV of the coil, but also facilitated displacement currents near the base of the skull and cerebellum, both inherently further from the coil. Although our study demonstrated an improvement in coil sensitivity for a specific commercial head coil (1 transmit/24 channel receive, Nova Medical), recent investigations have shown that a newer version (1 transmit/32 channel, Nova Medical) also suffered from poor coil sensitivity for inferior regions of the head with demonstrated improvements in whole brain diffusion when HPM pads were placed near the temporal lobes and neck (16).

There are some limitations to this work. The thickness of the HPM pads used in this work was 2 cm, which occupied a substantial amount of space inside the head coil. This spacing was maintained in the case without HPM by using cushions that were approximately of the same height. Relative permittivities considered in this work were limited to 110 and 300, which are known to be achievable with either barium titanate or calcium titanate powder and heavy water. In principle a combination of the two powders could be used to achieve intermediate values, and could be explored in future work. Thinner HPM pads with different properties and dimensions (23,35) may also improve performance while providing more space inside the head coil. The dimensions of the HPM pads, additionally, changed in shape during in-vivo experiments, because of the subject’s head resting on the pads. Alternative methods of building HPM pads, such as using hydroxyl-ethyl cellulose gel (27) or sintered ceramic based HPM (38,39) to improve mechanical stability over time may benefit future studies. Additionally, in this study we performed simulations with only one head model, which was not based on any of the subjects in experiment. However, even considering an additional safety factor of two to account for variability in head anatomies (40) the recommended limits for SAR would not be exceeded in the fMRI sequence we used. Furthermore, if available, a different head coil with better initial transmit efficiency in the cerebellum might not benefit from use of HPM for improved detection of fMRI in the manner used here. Finally, order of conditions (with or without HPM pads) were not randomized between subjects, since the input transmit voltage for each subject was set for the case without HPM pads (carried out first). Since the group analysis showed an improvement in functional activation in regions near the HPM pad and not in superior regions of the brain, we expect that randomizing the conditions would not result in a significant difference.

In conclusion, our work demonstrates a relatively inexpensive method to improve cerebellar fMRI signal at 7T using HPM pads to extend the coil sensitivity outside of an existing commercial head coil. Safety assessments carried out in simulations showed that local and

global SAR did not exceed current regulatory limits. For this particular arrangement, the simulation and experimental results showed an improvement in transmit efficiency and SNR, particularly in the cerebellum and regions inferior to the base of the skull, which was utilized for improving detection of functional BOLD activation in the cerebellum for a motor task. Individual as well as group analyses demonstrated a statistically significant increase in the functional activation in the cerebellum, which was proximal to the position of the HPM pads. This method could increase the utility of existing commercial head coils at 7T for whole brain fMRI and other applications.

Acknowledgments

The authors would like to thank Dr. Ryan Brown for discussions regarding experimental RF data and background literature, and Dr. Yagna Pathak for discussions regarding FEAT FSL.

GRANT SUPPORT: This work was supported in part by NSF 1453675, NIH R01 EB002568, NIH R01 EB011551, NIH R01 EB021277 and was performed under the rubric of the Center for Advanced Imaging Innovation and Research (CAI^{2}R, www.cai2r.net), an NIBIB Biomedical Technology Resource Center (NIH P41 EB017183).

References

1. Ogawa S, Lee TM, Kay AR, Tank DW. Brain magnetic resonance imaging with contrast dependent on blood oxygenation. Proceedings of the National Academy of Sciences. 1990; 87(24):9868–9872.
2. DeYoe EA, Bandettini P, Neitz J, Miller D, Winans P. Functional magnetic resonance imaging (FMRI) of the human brain. Journal of Neuroscience Methods. 1994; 54(2):171–187. [PubMed: 7869750]
3. Biswal B, Zerrin Yetkin F, Haughton VM, Hyde JS. Functional connectivity in the motor cortex of resting human brain using echo-planar mri. Magnetic Resonance in Medicine. 1995; 34(4):537–541. [PubMed: 8524021]
4. Stoodley CJ, Schmahmann JD. Functional topography in the human cerebellum: A meta-analysis of neuroimaging studies. NeuroImage. 2009; 44(2):489–501. [PubMed: 18835452]
5. Stoodley CJ, Valera EM, Schmahmann JD. Functional topography of the cerebellum for motor and cognitive tasks: An fMRI study. NeuroImage. 2012; 59(2):1560–1570. [PubMed: 21907811]
6. Hui KKS, Liu J, Marina O, et al. The integrated response of the human cerebro-cerebellar and limbic systems to acupuncture stimulation at ST 36 as evidenced by fMRI. NeuroImage. 2005; 27(3):479–496. [PubMed: 16046146]
7. Stoodley CJ, Schmahmann JD. Evidence for topographic organization in the cerebellum of motor control versus cognitive and affective processing. Cortex. 2010; 46(7):831–844. [PubMed: 20152963]
8. Okada T, Yamada H, Ito H, Yonekura Y, Sadato N. Magnetic field strength increase yields significantly greater contrast-to-noise ratio increase: Measured using BOLD contrast in the primary visual area1. Academic Radiology. 2005; 12(2):142–147. [PubMed: 15721590]
9. van der Zwaag W, Francis S, Head K, et al. fMRI at 1.5, 3 and 7 T: Characterising BOLD signal changes. NeuroImage. 2009; 47(4):1425–1434. [PubMed: 19446641]
10. Beisteiner R, Robinson S, Wurnig M, et al. Clinical fMRI: Evidence for a 7 T benefit over 3 T. NeuroImage. 2011; 57(3):1015–1021. [PubMed: 21620980]
11. Küper M, Thürling M, Stefanescu R, et al. Evidence for a motor somatotopy in the cerebellar dentate nucleus—An FMRI study in humans. Human Brain Mapping. 2012; 33(11):2741–2749. [PubMed: 21938757]
12. Keltner JR, Carlson JW, Roos MS, Wong ST, Wong TL, Budinger TF. Electromagnetic fields of surface coil in vivo NMR at high frequencies. Magnetic Resonance in Medicine. 1991; 22(2):467–480. [PubMed: 1812380]

13. Vaughan JT, Garwood M, Collins CM, et al. 7T vs. 4T: RF power, homogeneity, and signal-to-noise comparison in head images. Magnetic Resonance in Medicine. 2001; 46(1):24–30. [PubMed: 11443707]
14. Vaidya MV, Collins CM, Sodickson DK, Brown R, Wiggins GC, Lattanzi R. Dependence of B1+ and B1- Field Patterns of Surface Coils on the Electrical Properties of the Sample and the MR Operating Frequency. Concepts in magnetic resonance Part B, Magnetic resonance engineering. 2016; 46(1):25–40. [PubMed: 27795697]
15. Teeuwisse WM, Collins CM, Wang C. , et al. Improvement in high field pulsed arterial spin labeling using dielectric pads: a simulation and experimental study. Proceedings of the International Society for Magnetic Resonance in Medicine; Stockholm. May 2010; 3863
16. Vu AT, Auerbach E, Lenglet C, et al. High resolution whole brain diffusion imaging at 7 T for the Human Connectome Project. NeuroImage. 2015; 122:318–331. [PubMed: 26260428]
17. Foo TK, Hayes CE, Kang YW. Reduction of RF penetration effects in high field imaging. Magnetic Resonance in Medicine. 1992; 23(2):287–301. [PubMed: 1549043]
18. Alsop DC, Connick TJ, Mizsei G. A spiral volume coil for improved RF field homogeneity at high static magnetic field strength. Magnetic Resonance in Medicine. 1998; 40(1):49–54. [PubMed: 9660552]
19. Yang QX, Mao W, Wang J, et al. Manipulation of image intensity distribution at 7.0 T: passive RF shimming and focusing with dielectric materials. Journal of magnetic resonance imaging : JMRI. 2006; 24(1):197–202. [PubMed: 16755543]
20. Sreenivas M, Lowry M, Gibbs P, Pickles M, Turnbull LW. A simple solution for reducing artefacts due to conductive and dielectric effects in clinical magnetic resonance imaging at 3 T. European Journal of Radiology. 2007; 62(1):143–146. [PubMed: 17169519]
21. Webb AG. Dielectric Materials in Magnetic Resonance. Concept Magn Reson A. 2011; 38A(4): 148–184.
22. Haines K, Smith NB, Webb AG. New high dielectric constant materials for tailoring the B1+ distribution at high magnetic fields. Journal of magnetic resonance. 2010; 203(2):323–327. [PubMed: 20122862]
23. Teeuwisse WM, Brink WM, Haines KN, Webb AG. Simulations of high permittivity materials for 7 T neuroimaging and evaluation of a new barium titanate-based dielectric. Magnetic Resonance in Medicine. 2012; 67(4):912–918. [PubMed: 22287360]
24. Snaar JEM, Teeuwisse WM, Versluis MJ, et al. Improvements in high-field localized MRS of the medial temporal lobe in humans using new deformable high-dielectric materials. NMR in biomedicine. 2011; 24(7):873–879. [PubMed: 21834010]
25. Teeuwisse WM, Brink WM, Webb AG. Quantitative assessment of the effects of high-permittivity pads in 7 Tesla MRI of the brain. Magnetic Resonance in Medicine. 2012; 67(5):1285–1293. [PubMed: 21826732]
26. O'Brien KR, Magill AW, Delacoste J, et al. Dielectric pads and low- B1+ adiabatic pulses: Complementary techniques to optimize structural T1w whole-brain MP2RAGE scans at 7 tesla. Journal of Magnetic Resonance Imaging. 2014; 40(4):804–812. [PubMed: 24446194]
27. O'Reilly TP, Webb AG, Brink WM. Practical improvements in the design of high permittivity pads for dielectric shimming in neuroimaging at 7T. Journal of magnetic resonance. 2016; 270:108–114. [PubMed: 27434779]
28. Christ A, Kainz W, Hahn EG, et al. The Virtual Family—development of surface-based anatomical models of two adults and two children for dosimetric simulations. Physics in Medicine & Biology. 2010; 55(2):N23. [PubMed: 20019402]
29. Food and Drug Administration. Criteria for Significant Risk Investigations of Magnetic Resonance Diagnostic Devices - Guidance for Industry and Food and Drug Administration Staff. Jun 13.2014
30. International Electrotechnical Commission. Medical electrical equipment - Part 2-33: Particular requirements for the basic safety and essential performance of magnetic resonance equipment for medical diagnosis. 2010IEC 60601-2-33 ed30
31. Collins CM, Li S, Smith MB. SAR and B1 field distributions in a heterogeneous human head model within a birdcage coil. Magnetic Resonance in Medicine. 1998; 40(6):847–856. [PubMed: 9840829]

32. Klose U. Mapping of the radio frequency magnetic field with a MR snapshot FLASH technique. Medical Physics. 1992; 19(4):1099–1104. [PubMed: 1518473]

33. Kellman P, McVeigh ER. Image reconstruction in SNR units: a general method for SNR measurement. Magnetic Resonance in Medicine. 2005; 54(6):1439–1447. [PubMed: 16261576]

34. Yang QX, Wang J, Wang J, Collins CM, Wang C, Smith MB. Reducing SAR and enhancing cerebral signal-to-noise ratio with high permittivity padding at 3 T. Magnetic Resonance in Medicine. 2011; 65(2):358–362. [PubMed: 21264928]

35. Brink WM, Webb AG. High permittivity pads reduce specific absorption rate, improve B1 homogeneity, and increase contrast-to-noise ratio for functional cardiac MRI at 3 T. Magnetic Resonance in Medicine. 2014; 71(4):1632–1640. [PubMed: 23661547]

36. Collins CM, Carluccio G, Vaidya MV. , et al. High-permittivity Materials can Improve Global Performance and Safety of Close-Fitting Arrays. Proceedings of the 22nd Annual Meeting of the International Society for Magnetic Resonance in Medicine; Milan. 2014. 0404

37. Stefanescu MR, Thürling M, Maderwald S, et al. A 7T fMRI study of cerebellar activation in sequential finger movement tasks. Experimental Brain Research. 2013; 228(2):243–254. [PubMed: 23732948]

38. Luo W, Lanagan MT, Sica CT, et al. Permittivity and performance of dielectric pads with sintered ceramic beads in MRI: early experiments and simulations at 3 T. Magnetic Resonance in Medicine. 2013; 70(1):269–275. [PubMed: 22890908]

39. Koolstra K, Börnert P, Brink W, Webb A. Improved image quality and reduced power deposition in the spine at 3 T using extremely high permittivity materials. Magnetic Resonance in Medicine. 2017 early view.

40. de Greef M, Ipek O, Raaijmakers AJE, Crezee J, van den Berg CAT. Specific absorption rate intersubject variability in 7T parallel transmit MRI of the head. Magnetic Resonance in Medicine. 2013; 69(5):1476–1485. [PubMed: 22760930]

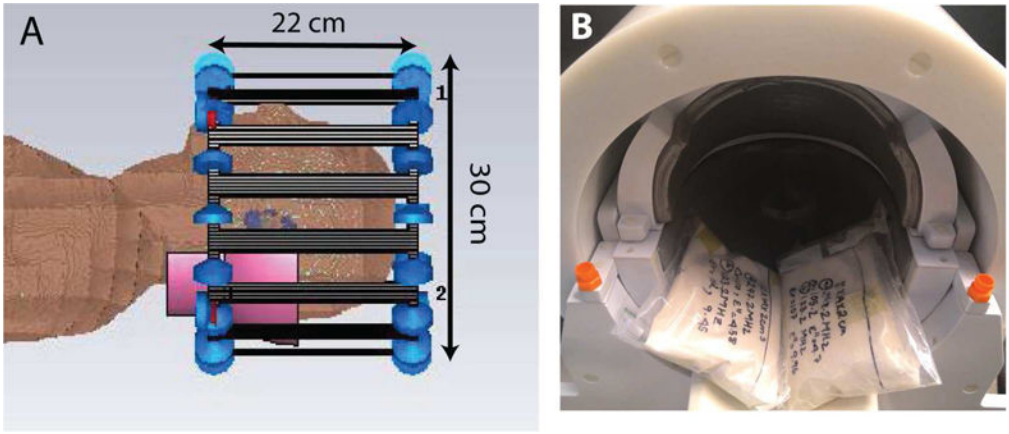

Figure 1.

Configurations of birdcage coil, HPM pads, and head model in simulation (A) and of pads in head coil in experiment (B). The dimensions of the birdcage model in simulation approximated the dimensions of the transmit coil in experiment. HPM pads are shown in pink in the simulation setup and white in the experimental setup. Experimental setup is shown before positioning the volunteer in the head coil.

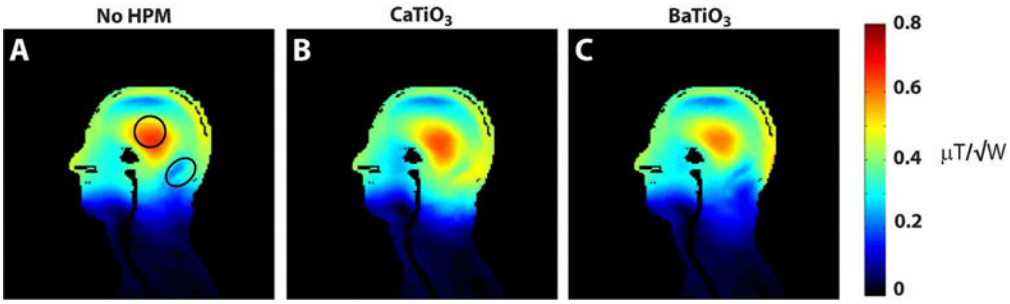

Figure 2.

Transmit efficiency in simulation. Simulated |B1+| maps were normalized by the square root of the input power. CaTiO3 HPM pads (B) improved transmit efficiency in deep, inferior regions of the head including the cerebellum when compared to the cases with no HPM (A) and BaTiO3 HPM pads (C). Average |B1+| values in the central ROI (no HPM: 0.55, CaTiO3: 0.51) and cerebellum ROI (no HPM: 0.29, CaTiO3: 0.44) were used to scale simulated peak 10g SAR and Head SAR shown in Table 1.

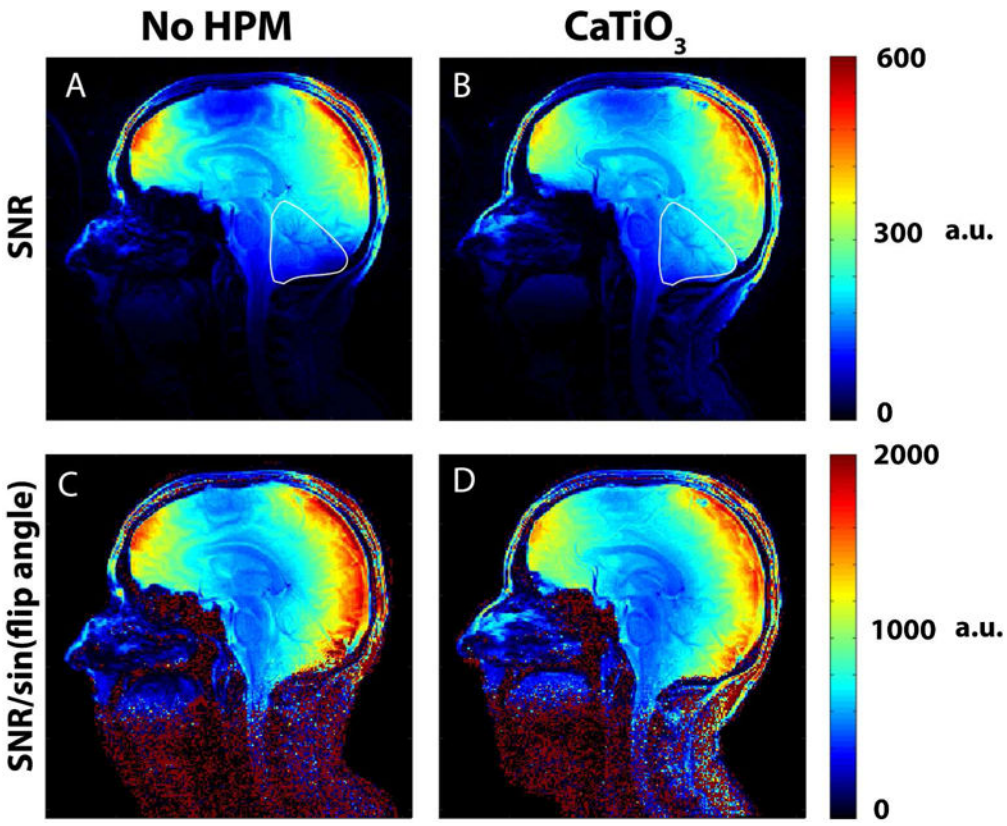

Figure 3.

Experimental SNR maps for one subject show that placing pads of CaTiO3 slurry at the back of the neck extends the sensitivity of the coil and improves SNR in the cerebellum, neck muscles, brainstem, and superior spinal cord. An SNR improvement of 26.79 % with HPM (B vs. A) was obtained for the cerebellum in the image shown, outlined in white. SNR maps normalized by the corresponding flip angle maps obtained during the same session show a decrease in receive-only sensitivity by 7.27 % (D vs. C) in the same ROI, demonstrating that the improvement in SNR observed is primarily due to an increase in flip angle (38.67 % increase with HPM) in the ROI.

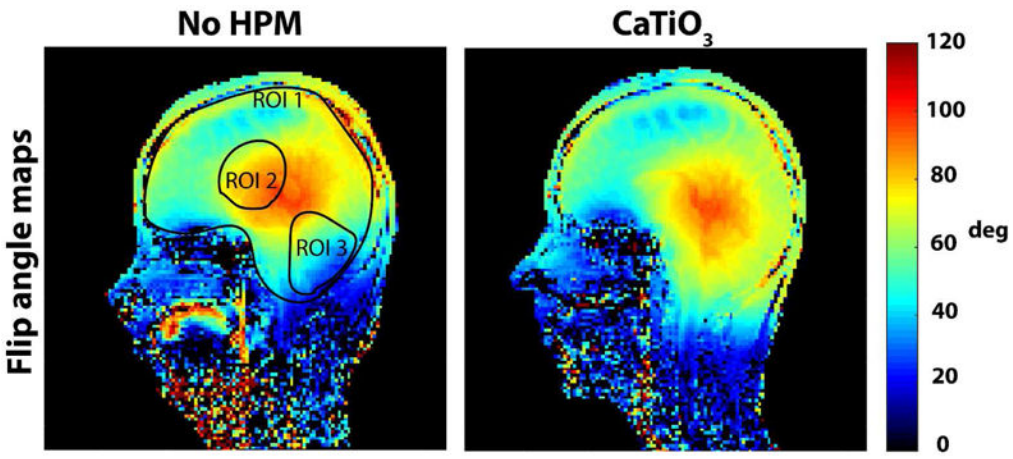

Figure 4.

Experimental flip angle maps show an improvement with HPM pads in the inferior regions of the brain, and match the trend of the simulated transmit efficiency maps (Fig 2). Mean flip angle across all subjects (with/without HPM: ROI 1: 67.70 ± 4.55/67.86 ± 7.23, ROI 2: 86.37 ± 5.99/89.45 ± 3.64, ROI 3: 68 ± 10.52/51.06 ± 8.65, where variability is measured using the standard deviation) show an improvement in the cerebellum by 33 %.

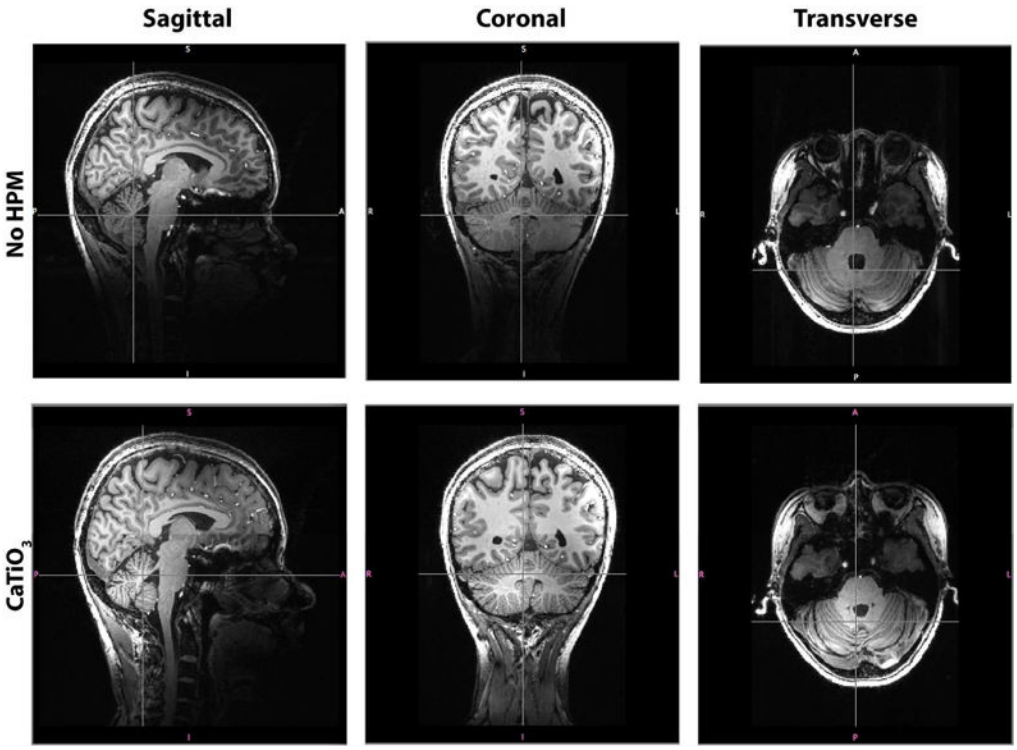

Figure 5.

T_1-weighted MPRAGE images (sagittal, coronal and transverse slices) show signal and contrast improvement in the superior regions of the neck and inferior regions of the brain and brainstem when using $CaTiO_3$ pads. In particular, the cerebellum, neck muscles, brainstem, and spinal cord are more clearly visible in the presence of $CaTiO_3$ pads.

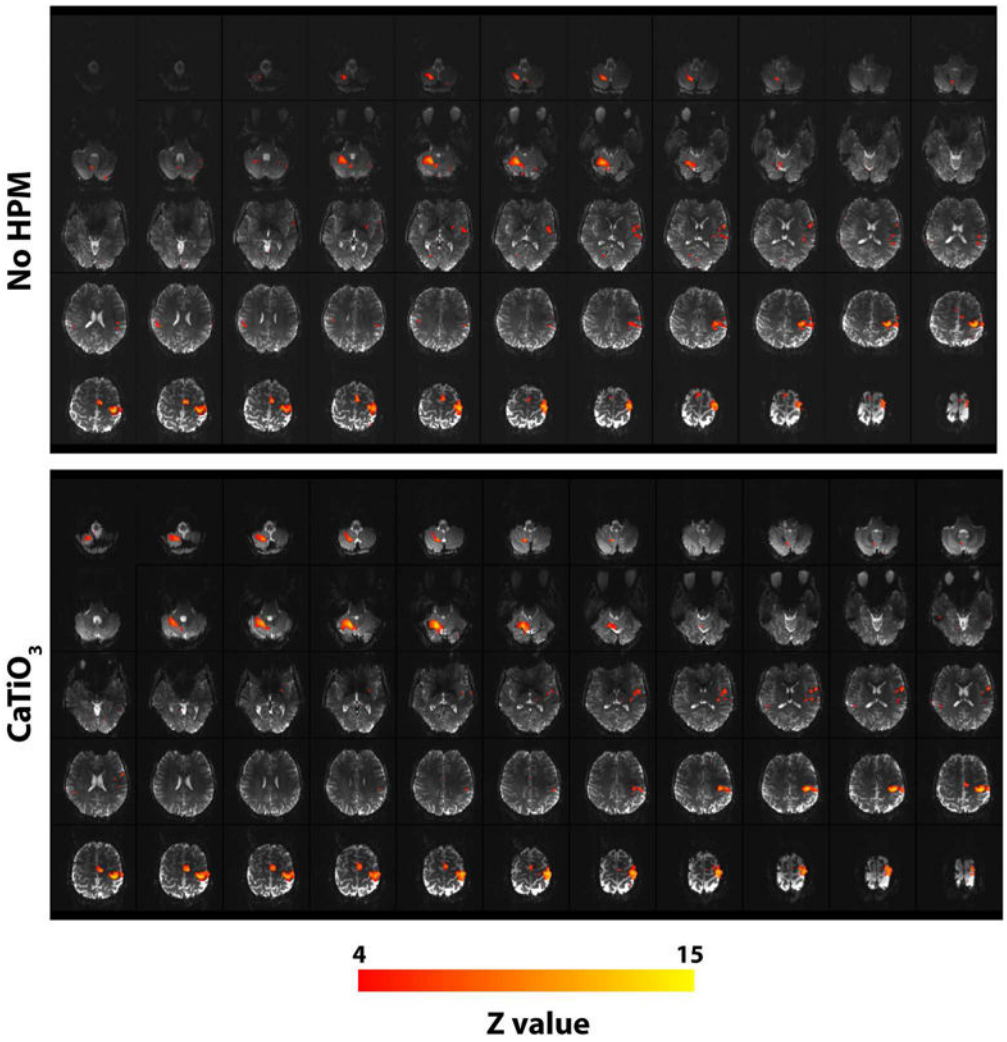

Figure 6.

Functional activation maps (shown for Z >=4) overlaid on structural echo-planar images for one volunteer show an improvement in both signal and functional activation in the inferior axial slices of the cerebellum with HPM pads. No significant difference is seen for the superior slices of the brain. Functional activation, for right hand finger tapping, shows contralateral activation in the motor cortex and an ipsilateral activation in the cerebellar cortex.

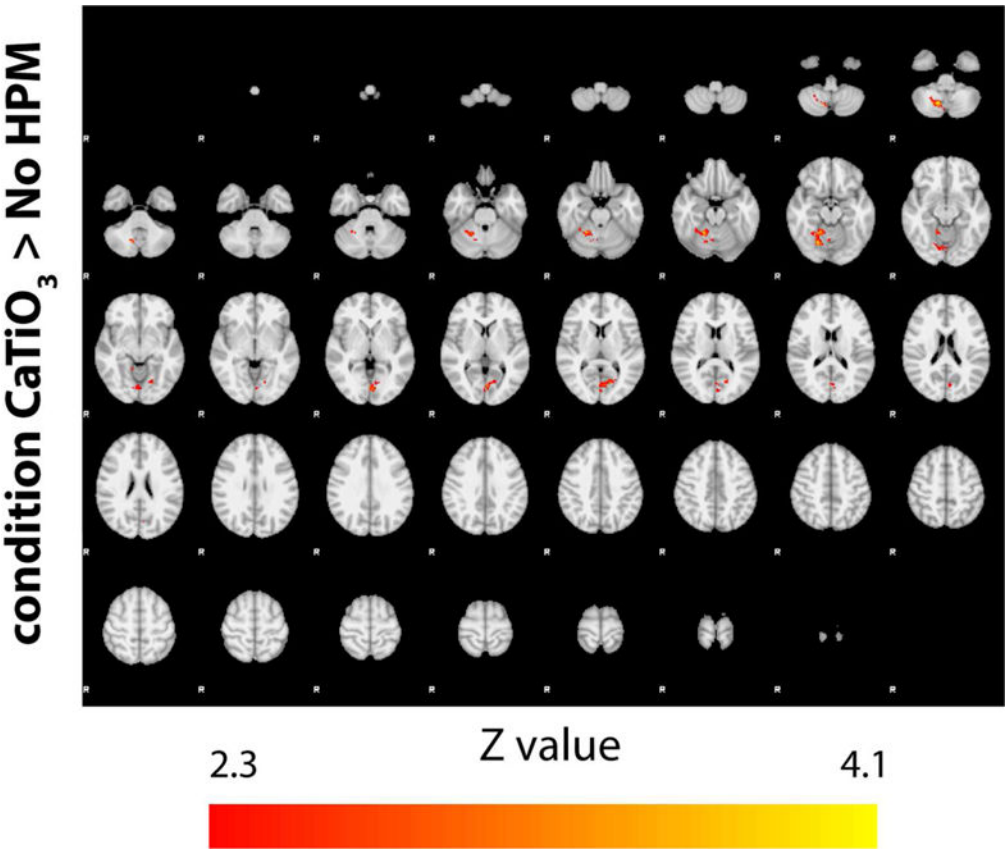

Figure 7.

Higher-level statistical comparison of activation patterns (shown for Z>=2.3) in the presence of HPM pads across all subjects. Use of HPM pads results in notable increase in activation in the cerebellar cortex (condition $CaTiO_3$> no HPM). No significant increase in activation was observed in the absence of HPM pads, i.e., condition no HPM> $CaTiO_3$, (data not shown).

Table I

Peak local 10g SAR and Head average SAR values obtained from simulations for the experimental EPI sequence with 90° excitation either in the center of the head or in the cerebellum.

	With 90° in center		With 90° in cerebellum	
	Peak 10g SAR	**Head Average SAR**	**Peak 10g SAR**	**Head Average SAR**
No HPM	0.93	0.30	3.37	1.08
With HPM	1.18	0.38	1.61	0.51
% increase w/HPM	27	27	−52	−53

Table II

Maximum Z value and total number of activated voxels (Z>=6) for cluster sizes with greater than two voxels in the cerebellum for all subjects

Subject	Total voxels		Maximum Z value	
	no HPM	$CaTiO_3$	no HPM	$CaTiO_3$
1	802	745	14.2	14.3
2	240	312	9.89	11.9
3	195	290	12.4	13.2
4	94	238	10.7	13
5	675	1114	15	15.9
6	315	495	11.9	13.8
7	226	257	11.5	11.4
8	207	435	13.2	14.2